

Level-aware Haze Image Synthesis by Self-Supervised Content-Style Disentanglement

Chi Zhang*, *Member, IEEE*, Zihang Lin*, Liheng Xu, Zongliang Li, Le Wang, *Senior Member, IEEE*, Yuehu Liu, *Member, IEEE*, Gaofeng Meng, *Senior Member, IEEE*, Li Li, *Fellow, IEEE* and Nanning Zheng, *Fellow, IEEE*

Abstract—The key procedure of haze image translation through adversarial training lies in the disentanglement between the feature only involved in haze synthesis, i.e. **style feature**, and the feature representing the invariant semantic content, i.e. **content feature**. Previous methods separate content feature apart by utilizing it to classify haze image during the training process. However, in this paper we recognize the incompleteness of the content-style disentanglement in such technical routine. The flawed style feature entangled with content information inevitably leads the ill-rendering of the haze images. To address, we propose a self-supervised style regression via stochastic linear interpolation to reduce the content information in style feature. The ablative experiments demonstrate the disentangling completeness and its superiority in level-aware haze image synthesis. Moreover, the generated haze data are applied in the testing generalization of vehicle detectors. Further study between haze-level and detection performance shows that haze has obvious impact on the generalization of the vehicle detectors and such performance degrading level is linearly correlated to the haze-level, which, in turn, validates the effectiveness of the proposed method.

Index Terms—Haze Synthesis, Unsupervised Image-to-image Translation, Self-supervised Disentanglement.

1 INTRODUCTION

FOG and haze brings huge troubles to the driving safety of vehicles, especially for autonomous vehicles equipped with color cameras and LiDARs. Image data collected by sensors degrade heavily due to the dense-distributed atmospheric suspended particulates. However, since the foggy and hazy weather is rare, temporary and hard to forecast, there exists limited samples of diverse concentration level under such scenarios. As a result, there lacks sufficient data for autonomous perception, especially when testing its generalization in terms of the haze weather.

In order to complement haze images for testing, a common practice is to synthesize them from clear images and corresponding depth maps under haze image formation model. Many sophisticated hand-crafted methods like [1] [2] exploit or calculate depth map to estimate the atmosphere transmittance (scattering ability of suspended particles) in the environment. In this circumstance, the quality of synthesized images depends on the accuracy of depth prediction to some extent. However, compared with color images, depth images acquired by professional equipment are often noisy and discontinuous [3] [4]. On the other hand, the process of depth prediction will bring in extra error. Such inherent defects make traditional algorithms mentioned above hard to break through the bottleneck of haze image synthesis. Inspired by previous work [5]–[9] which explore how to transform weather condition

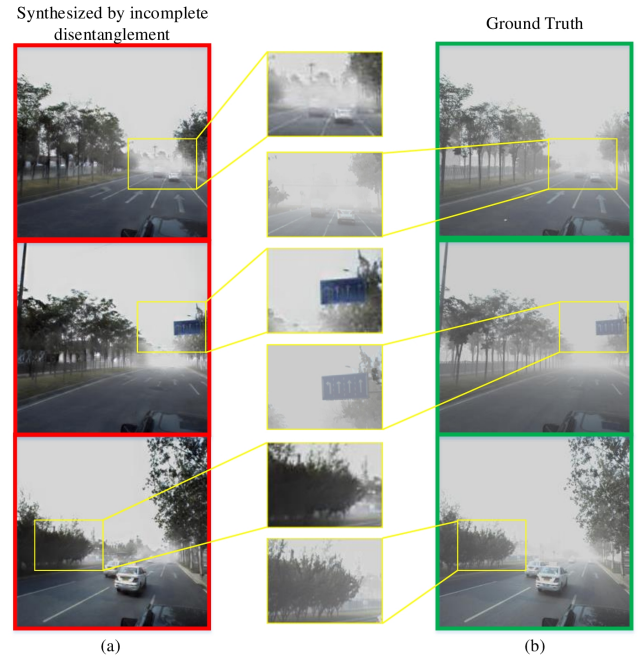


Fig. 1: Examples of unreal haze images caused by incomplete disentanglement. (a) represents haze images generated by methods when potential content information remaining in separated style feature. As the picture of top row shows, rendered haze simply appears abruptly like a puff of smoke in the road while haze in corresponding ground truth images (b) is evenly distributed according to depth and semantic content. Besides, some objects such as signs and trees in the middle and bottom respectively are excluded from haze. Such uneven distribution makes generated images look factitious.

between image domains using generative adversarial networks, the generation of haze images can also borrow the idea of image

- *Equal contribution.
- This work was supported by the National Natural Science Foundation of China under Grant 61973245 and 61976171. Yuehu Liu is the corresponding author. E-mail: liuyh@xjtu.edu.cn.
- Chi Zhang, Zihang Lin, Liheng Xu, Zongliang Li, Le Wang, Yuehu Liu and Nanning Zheng are with the Institute of Artificial Intelligence and Robotics, Xi'an Jiaotong University, Xi'an, China.
- Gaofeng Meng is with National Laboratory of Pattern Recognition, Institute of Automation, Chinese Academy of Sciences, Beijing 100190, China.
- Li Li is with Department of Automation, BNRist, Tsinghua University, Beijing, China 100084.

translation which performs style transform between haze domain and haze-free domain.

Theoretically, it is nearly impossible to obtain one-to-one paired training images required for supervised image translation algorithms because there exists either haze or haze-free weather in a particular scene at one time. Instead, such problem is posed as unsupervised image translation which does not require a one-to-one correspondence. For a pair of haze image and clear image represent the same scene, they are assumed to be disentangled into the feature only involved in haze synthesis, i.e. *style feature* and the feature representing the invariant semantic content, i.e. *content feature*. Commonly, existing image translation methods decouple image content and style feature and introduce strict constraints to guarantee the absolute separateness of style information from content feature. Nevertheless, potential content information remaining in style feature is ignored, which degrades the synthesized image in terms of photorealism. As shown in Fig. 1, due to such incomplete disentanglement, rendered haze simply appears abruptly like a puff of smoke covering the end of the road which looks factitious. Moreover, haze images simply generated by such image translation lack for diversity since the network is unaware of the haze level.

In this paper, we address the synthesis issues on fore-mentioned disentangling completeness and level-aware diversity. Benefited from disentangled representation learning, we extract the content feature of a haze-free image and then combine it with the style feature of a haze image to synthesize the corresponding haze image. Different from [10] [11], we not only introduce the content discriminator to supervise the upgrading of content encoder, but also apply the regularization of level-aware style feature regression to suppress potential content information in extracted haze feature. Taking advantage of the level-variability of haze and the immutability of content, such process is made self-supervised via randomly linear interpolation of style feature. Our empirical studies on feature disentanglement proves that we successfully disentangle style features and content features. After mapping the style feature to the linear space, we successfully generate multi-level haze images by manipulating the style feature. Finally, to demonstrate that the haze images generated by our method provide sufficient and effective difficult scenario data support for the scenario test of the autonomous driving perception module, we set up the experiment of worst perception scenario (WPS) search with controllable haze density for controlling the difficulty of scenario. Results indicate that haze level is highly correlated with scene difficulty, which further clarify the necessity of testing self-driving car under multi-level haze weather and our framework can replenish the rare haze data.

There are three contributions of this paper:

1. We propose the self-supervised style regression to suppress content information in style feature.
2. By mapping the style feature to the linear space, we expand the domain into a continuous space and present a level-aware disentangling framework in the unsupervised image-to-image translation to produce multi-level haze images.
3. Based on our unsupervised framework which enables the synthesis of diversity-controllable haze images, we quantitatively prove that traffic scenes become worse in haze weather by proceeding online searching of worst haze scenario.

2 RELATED WORK

The method in this paper benefits from traditional haze image synthesis methods and disentangled image representation learning. Therefore, this section mainly introduces the related work of haze image generation method and disentangled representation learning.

2.1 Atmospheric Scattering Model and Haze Image Generation

The atmospheric scattering model is an important model to describe the synthesis of haze images, and its formal description is as follows:

$$I(x) = J(x)t(x) + A(1 - t(x)) \quad (1)$$

where $I(x)$ represents the haze image collected by the camera and $J(x)$ denotes real reflected light on the surface of objects (normal image). $t(x)$ is the medium transmittance and A is the atmospheric light intensity. x represents pixel. Given the image depth $d(x)$ and the atmospheric scattering coefficient β , transmittance $t(x)$ can be calculated as $t(x) = e^{-\beta d(x)}$.

Therefore, the key to generating a haze image is how to estimate the depth image of a single haze-free image, and then forecast the atmospheric transmittance (scattering ability of suspended particles) in the imaging environment. Zhuo et al. estimated the defocus map of a single image by propagating the amount of defocus blur at the edge of the image to the entire image and calculate the depth estimation of a single image [12]. However, since it is impossible to accurately determine whether the blur at the edge of the image is caused by the defocus of the device or the imaging problem of the device, this method has a large error in reckoning the amount of defocus blur. In 2015, Sun et al. simulated the haze under different visibility [1]. Although they based on the single image defocus map estimation algorithm principle of atmospheric scattering, the over-simplification of smog cannot generate the randomness and variability of smog in nature due to the simplicity of the calculation process. Wang et al. explored haze simulation for realistic scene rendering and animation [?]. With the same purpose of rendering realistic haze scene, Guo et al. proposed a new rendering method based on transmission map estimation [13]. Then took advantage of the Markov random field model and the bilateral filter to estimate the transmission map and virtual foggy scenes were realistically rendered with the generated perlin noise image and the transmission map according to the atmospheric scattering model. Nevertheless, compared to ordinary RGB images, depth images are more difficult to acquire. Besides, the quality of the composite image depends on the quality of the depth image, which leads to the existence of obviously unreal parts in the composite image.

On the other hand, thanks to the development of deep neural networks and generative adversarial networks (GAN), the data-driven smog image generation method is to mine the mapping relationship between haze-free traffic scene images and haze images through GAN. Its essence is an image translation model, the purpose of which is to map the image in one domain to the corresponding image [5] in another domain. Image translation problems can be trained in a supervised or unsupervised manner. The “Pix2Pix” framework proposed by Isola et al. is trained in a supervised manner, using conditional GAN to learn the mapping between the input image domain and the output image domain [5]. Unsupervised image translation models require only

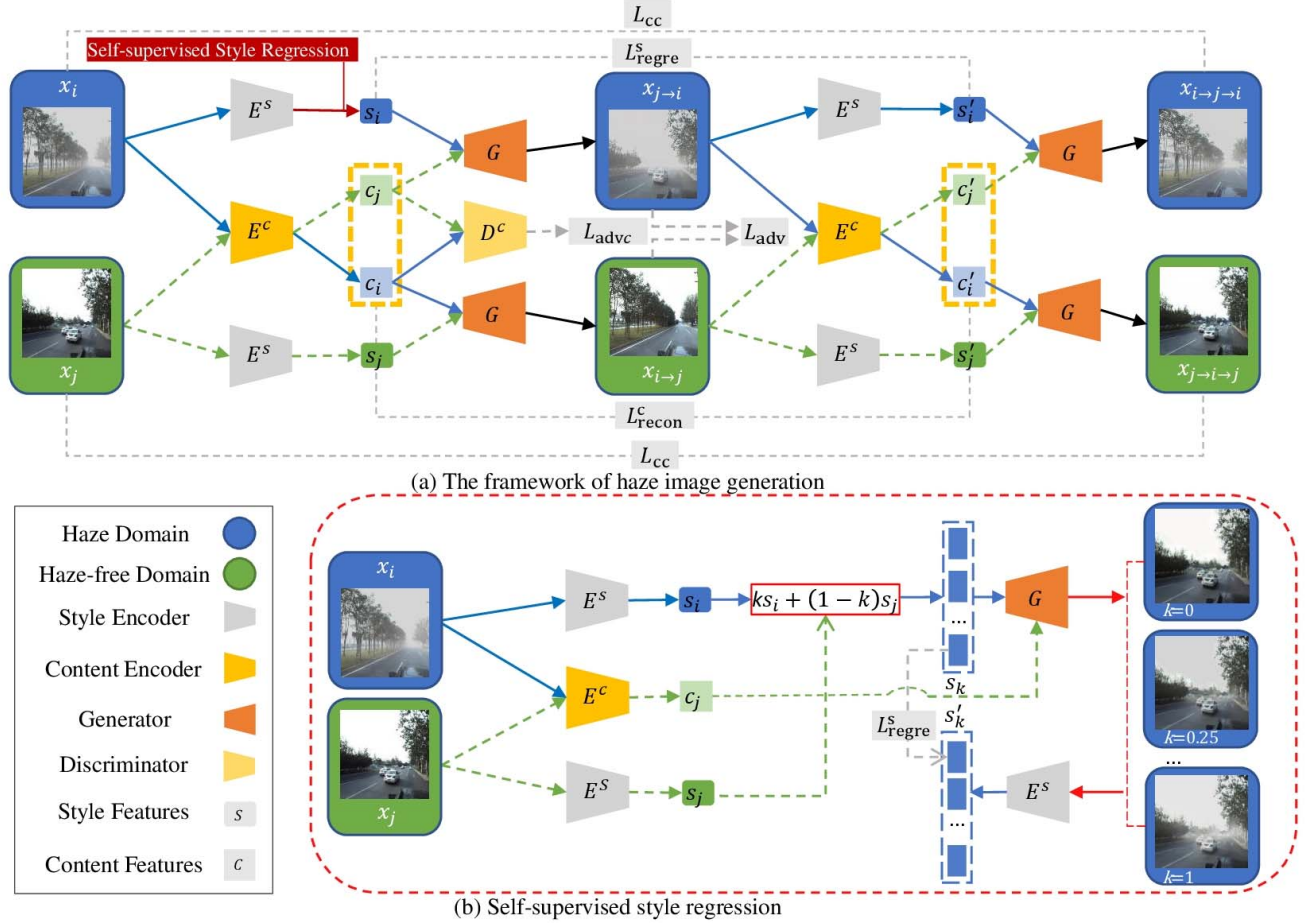


Fig. 2: The overall framework of our multi-level haze image generation model. (a) shows the process of haze image generation. To ensure the quality of output images, we employ cycle-consistency in our model. We also put content feature of each domain into a content discriminator in order to train the content encoder. Based on our assumption, our goal is to induce the discriminator to be confused when confronted with content feature since it contains no domain-respective information. (b) Inspired by the level-variability of style feature, we interpolate style feature with parameter k to make the upgrading of style encoder self-supervised and trained the end to end producing model level-aware.

two sets of independent images, that is, learning the mapping between the two image domains. Because training data is easier to obtain, unsupervised image translation models are more widely used. The problem of unsupervised image translation is an ill-posed problem that requires more constraints for solving. The cycle consistency constraint proposed in CycleGAN is the most widely used constraint [6]. In addition to one-to-one mapping, MUNIT [8] and BicyclGAN [14] proposed multimodal generative models to achieve one-to-many mapping, which means multiple images of the target image domain corresponding to the input image can be generated. StarGAN [15] and UDFN [16] further implement image mapping between multiple image domains. Use the unsupervised image translation model to directly learn the mapping between the haze-free image and the haze image, so as to realize the haze image generation. Although these general image translation models can realize the mapping between haze-free images and haze images, the disentanglement of content features and haze features often results in changes in content, which cannot meet the requirements. Therefore, this paper uses the disentangled content and haze features to ensure the consistency of content of generated images and input images.

2.2 Disentangled Representation Learning

Disentangled representation learning is to model the factors that cause the data to change and to acquire interpretable variables which can be identified and disentangled. Mathieu combined variational autoencoders and conditional GAN and disentangled the representation of data into two categories: category-related and category-independent in a weakly supervised learning way [17]. Recently, researchers have proposed unsupervised disentangled representation learning. By maximizing the mutual information between hidden variables and data variables, InfoGAN achieved the unsupervised disentangled representation learning [18]. Instead, DrNet used the viewpoint correlation of the video and adversarial loss to decouple the characterization of the video frame as time-independent content part and time-related pose part [11] while DRIT used content adversarial loss to disentangle images into domain-invariant and domain-specific representations [10]. However, the content confrontation loss can only suppress the style information in content features, and cannot guarantee that there is no content information in style features. Therefore, on the basis of the domain against classifier and content adversarial losses, the KL loss is used to constrain the distribution of the haze feature to suppress the content information in haze features.

3 METHOD

Partially-shared latent space assumption is common in disentangled representation learning tasks like [10], which suppose that images from different domains share one content space while keep style space domain-specific. These tasks often focus on style like sketch or photograph which are rendered directly on the spatial structure of an image without editing content. Oppositely, the style in our task is different level of haze leading to varying degree of scene blocks. Thin haze will slightly lower the visibility while thicker haze will almost block the disappearance point of the road. As mentioned before, the generation of haze is relatively concerned with the depth of scenes. In other words, we need information about scene structure to ensure produced haze match the correct spatial distribution. As a result, continuing to use domain-specified style encoders will bring the confusion about the spatial structure during the generation of haze, which is unwanted.

Inspired by [19], we not only align content but also style of two image domains to fully utilize all image samples. All encoders are domain-shared in our model. With the shared style encoder, the style encoder will learn to extract style feature on the premise of understanding the semantic structure. As a pair of haze image and clear image represent the same scene, we propose the follow proposition:

Proposition 1. *Images can be disentangled into shared content feature and style features.*

Based on proposition 1, we generate images by mixing content feature and style feature extracted by encoders. Concretely, we embed the input image into shared content feature space C and style feature space S . For a haze image x_i and a haze-free image x_j (unpaired, any haze image and haze-free image), we apply content encoder and style encoder to extract their content features and style features respectively:

$$\begin{aligned} c_i, s_i &= E^c(x_i), E^s(x_i), c_i \in C, s_i \in S_I \\ c_j, s_j &= E^c(x_j), E^s(x_j), c_j \in C, s_j \in S_J \end{aligned} \quad (2)$$

Fig. 2 (a) is the framework. The proposed model consists of three parts: 1) Encoders including the content encoder E^c and style encoder E^s . E^c and E^s are used to extract content and style features of both haze images and haze-free images respectively; 2) The only generator G generates corresponding images with content features and style features extracted by encoders as input; 3) The image discriminator D is used to distinguish real images from generated images and enhance the realism of output images. Since the two image domains share the same generator to generate haze images and haze-free images, the classifier D^{cls} is used to classify whether the generated image is a haze image or a haze-free image. The content discriminator D^c takes content features as input to classify whether the content feature originates from a haze image or a haze-free image.

3.1 Disentanglement of Content and Style

The so-called disentanglement of content and style means that the content feature contain no style information of the image and vice versa. The goal of a complete disentanglement is to ensure that both content and style features are extracted without other redundant information. On the one hand, we use a content discriminator to eliminate style information in content feature. On the other hand, we design the self-supervised style regression to suppress remaining content information in style feature.

3.1.1 Content Feature Discriminator

Similar to [10], we adopt the content feature discriminator D^c to guide the upgrading of content encoder. Theoretically, it is impossible to determine whether the image is from haze domain or haze-free domain based on the content feature since it contains no domain-related information.

At the first, we use the content encoder E^c to extract content features c_i, c_j of input pair x_i, x_j . Then input them into the content feature discriminator D^c to determine whether the input comes from a haze image or a haze-free image. E^c hopes to extract pure content features which can fool D^c while D^c will try to distinguish the specific categories of content features. Therefore, encoder E^c and discriminator D^c can iteratively evolve through adversarial training. Once the final balance is reached, it can be considered that the extracted content features do not contain any style information of the image. The specific loss function of content adversarial loss is as follows:

$$\begin{aligned} \mathcal{L}_{adv}(E^c, D^c) &= \mathbb{E}_{x_i} [\log(D^c(E^c(x_i)))] \\ &\quad + \mathbb{E}_{x_j} [\log(1 - D^c(E^c(x_j)))] \end{aligned} \quad (3)$$

D^c will try to maximize the above loss function to distinguish the source of input content features. Oppositely, E^c will try to minimize the above loss function to fool the content classifier. Ideally, after this game process reaches the Nash equilibrium, D^c cannot determine which image domain the content feature belongs to, which means that there is no haze information in the content feature. The disentanglement of style from content is successful once E^c only encodes the content feature of the image.

3.1.2 Self-supervised Style Feature Regression

The use of content feature discriminator and content adversarial classification loss can suppress style information in content features effectively. However, if there are no other constraints, there is no guarantee that the style features will not contain content information. As Fig. 1 shows, the trivial content information will disturb our controlling process just like noise. Thus in order to eliminate redundant content information in style features, we propose the self-supervised style regression as Fig. 2 (b) indicates.

Representing the style encoder by a non-linear function f . We firstly interpolate the style features extracted from the two images (x_i and x_j from haze and haze-free domain respectively) to obtain s_k :

$$s_k = kf(x_i) + (1 - k)f(x_j) \quad (4)$$

The purpose of interpolation is to force the extracted style feature to be linear. The manipulation on style space will be reflected in image space [27]. On this basis we have the following equation (Derive can be found in Appendix):

$$s_k = f(kx_i + (1 - k)x_j) \quad (5)$$

However, x_i and x_j have completely different content features and the content of the images obtained after linear interpolation will be an overlap of two images, which is nonsense. Theoretically, the style encoder will regard it as noise and eliminate it which leads to a pure style feature s_k . Then, we combine the content feature c_j with s_k and generate an image x_k with certain haze level between 0 and 1. Finally, the style feature of x_k is extracted (s'_k) and be aligned to s_k by minimizing Eq. 6:

$$\begin{aligned} \mathcal{L}_s(E^c, E^s, G) &= \\ \mathbb{E}_{x_i, x_j} [\|E^s(G(E^c(x_j), s_k)) - s_k\|_1] \end{aligned} \quad (6)$$

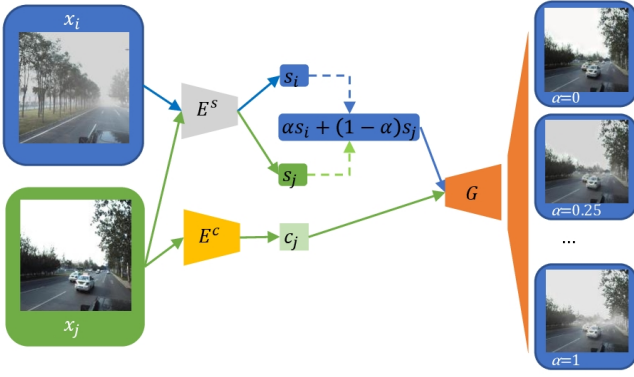


Fig. 3: Linear Style Manipulation. To generate traffic scenes with controllable haze level, we extract style features from two domains respectively and linear interpolate between them with parameter α . Higher α is equivalent to thicker haze. Then we combine the content feature and interpolated style feature to produce the corresponding haze scene image with α level of haze.

Without the monitoring from manual label, the whole process uses s_k as a pseudo label to self-supervise the upgrading of style encoder. Noted that this is not contradictory to our former statement about the necessity of understanding the spatial structure for style feature. Ideally, the extracted style should be able to understand the layout of traffic scenes so that generated haze will appear in correct place, but we do not want any traffic elements like cars or trees entangling with style feature.

Because of the random selecting of k when training, the network is forced to map haze-related style into the linear space. Therefore, we conduct linear manipulation on style feature and generate multi-level haze images like Fig. 3 shows.

Specifically, to generate an image x_α with a particular haze concentration of α for a certain scene, we extract the content feature c_j of the haze-free image x_j for that scene and combine it with the style feature s_α . s_α is α times s_i which refers to the haze of image x_i generated with β equals to 1 according to Eq. 1 and plus $(1 - \alpha)$ times s_j . The haze level is controlled by the scale factor α . As s_i is derived from the baseline haze, we can scale it up or down by α to obtain a scene specific image with the desired concentration of haze. The generating process can be illustrated by Eq. 7

$$x_\alpha = G(E^c(x_j), \alpha E^s(x_i) + (1 - \alpha)E^s(x_j)) \quad (7)$$

3.2 Loss Function

The overall loss function in this article contains the adversarial loss \mathcal{L}_{adv} , image reconstruction loss \mathcal{L}_{recon} , content reconstruction loss \mathcal{L}_{recon_c} , style regression loss \mathcal{L}_{regre} and cycle consistency loss \mathcal{L}_{cc} . The complete objective function is the weighted sum of all losses:

$$\mathcal{L} = \lambda_{adv}\mathcal{L}_{adv} + \lambda_{adv_c}\mathcal{L}_{adv_c} + \lambda_{recon}^x\mathcal{L}_{recon}^x + \lambda_{recon}^c\mathcal{L}_{recon}^c + \lambda_{regre}^s\mathcal{L}_{regre}^s + \lambda_{cc}\mathcal{L}_{cc} \quad (8)$$

Where $\mathcal{L}_{adv} = \mathcal{L}_{D_J} + \mathcal{L}_{D_I}$. \mathcal{L}_{D_J} and \mathcal{L}_{D_I} are adversarial losses in the haze and the haze-free domain, respectively. λ s are hyperparameters of the model which controls the importance of each loss item.

3.2.1 Adversarial Loss

Adversarial loss is applied in both the haze-free image domain and the haze image domain to ensure the authenticity of generated images. In the haze-free image domain, the adversarial loss is defined as follows:

$$\mathcal{L}_{D_J} = \mathbb{E}_{x_j \sim P_{X_J}} [\log D_J(x_j)] + \mathbb{E}_{x_i \sim P_{X_I}} [\log(1 - D_J(G(E^c(x_i), s_j)))] \quad (9)$$

The purpose of D_J is to distinguish between the real haze-free image and the generated dehazing image so D_J will try to maximize the above loss function. On the contrary, G_J will try to minimize it so as to make the generated dehazing image more realistic. Similarly, the adversarial loss \mathcal{L}_{D_I} in the haze image domain is:

$$\mathcal{L}_{D_I} = \mathbb{E}_{x_i \sim P_{X_I}} [\log D_I(x_i)] + \mathbb{E}_{x_j \sim P_{X_J}} [\log(1 - D_I(G(E^c(x_j), s_i)))] \quad (10)$$

We value the two adversarial loss as equally influential and simply add them up to build the final adversarial loss:

$$\mathcal{L}_{adv} = \mathcal{L}_{D_J} + \mathcal{L}_{D_I} \quad (11)$$

3.2.2 Reconstruction Loss and Style Regression Loss

Given the haze image and the haze-free image, the model should be able to reconstruct the input image after the processes of feature extraction and generation. Therefore, the distance between the reconstructed image and the original image is used as the reconstruction loss to further constrain the model:

$$\mathcal{L}_{recon}^x = \mathbb{E}_{x_i \sim P_{X_I}} [\|G(E^c(x_i), E^s(x_i)) - x_i\|_1] + \mathbb{E}_{x_j \sim P_{X_J}} [\|G(E^c(x_j), E^s(x_j)) - x_j\|_1] \quad (12)$$

Also, we want content and style features of decoded images are similar to original images as well. Consequently, we have reconstruction loss of content and style as below:

$$\mathcal{L}_{recon}^c = \mathbb{E}_{x_i \sim P_{X_I}} [\|E^c(G(E^c(x_i), E^s(x_i))) - E^c(x_i)\|_1] + \mathbb{E}_{x_j \sim P_{X_J}} [\|E^c(G(E^c(x_j), E^s(x_j)))) - E^c(x_j)\|_1] \quad (13)$$

$$\mathcal{L}_{recon}^s = \mathbb{E}_{x_i \sim P_{X_I}} [\|E_I^s(G(E^c(x_i), E^s(x_i)))) - E^s(x_i)\|_1] + \mathbb{E}_{x_j \sim P_{X_J}} [\|E_J^s(G(E^c(x_j), E^s(x_j)))) - E^s(x_j)\|_1] \quad (14)$$

Noted that we consider style reconstruction loss the same category as self-supervised style regression loss. We add them up with the same weight and get the style regression loss:

$$\mathcal{L}_{regre}^s = \mathcal{L}_{recon}^s + \mathcal{L}_s \quad (15)$$

3.2.3 Cross-cycle Consistency Loss

We also adopt the cross-cycle consistency loss [10] to learn the mapping between domains. For the generated haze image $x_{j \rightarrow i}$, the input haze-free image x_j can be obtained by dehazing conversion. The cross-cycle consistency loss limits the space of the generated image and preserves the content characteristics of the original input image. The l_1 distance between the cycle reconstructed image and the input image is used as the cross-cycle consistency loss. Forward translation process (mapping from haze image to haze-free image and vice versa):

$$x_{i \rightarrow j} = G(E^c(x_i), E^s(x_j)) \\ x_{j \rightarrow i} = G(E^c(x_j), E^s(x_i)) \quad (16)$$

Reverse translation process (reconstructing input image from generated image):

$$\begin{aligned} x_{i \rightarrow j \rightarrow i} &= G(E^c(x_{i \rightarrow j}), E^s(x_{j \rightarrow i})) \\ x_{j \rightarrow i \rightarrow j} &= G(E^c(x_{j \rightarrow i}), E^s(x_{i \rightarrow j})) \end{aligned} \quad (17)$$

The cross-cycle consistency loss in the haze image domain and the haze-free image domain is:

$$\begin{aligned} \mathcal{L}_{cc} &= \mathbb{E}_{x_i \sim P_{X_I}} [\|x_i - x_{i \rightarrow j \rightarrow i}\|_1] \\ &+ \mathbb{E}_{x_j \sim P_{X_J}} [\|x_j - x_{j \rightarrow i \rightarrow j}\|_1] \end{aligned} \quad (18)$$

4 EXPERIMENTS

In order to verify the effectiveness of the method in this paper, this section analyses the impact of different modules or losses on the generated results and compare them with existing methods quantitatively and qualitatively. This section first introduces datasets and implementation details of the method including the detailed introduction of the network structure and hyper-parameters. Then we will provide detailed analysis of our model including comparison with existing methods. Last part of this section are the ablation studies. The experimental hardware environment is NVIDIA TITAN XP GPU with 12GB of memory.

4.1 Dataset

The dataset is synthetic. Specifically, we use haze-free images (4000 images randomly selected) and corresponding depth images from the Apollo Space dataset [22] to synthesize haze images according to the atmospheric scattering model. For a given haze-free image and its depth image, we generate the corresponding haze image according to the equation 1. We randomly set atmospheric light intensity A from 0.8 to 1.0 and the value of atmospheric scattering coefficient β is 1. Finally, we select 1500 clear images and 1500 synthetic haze images as training data and 500 for each as test data.

4.2 Implementation Details

The network of our proposed model consists of a content encoder, a style encoder, a generator, a discriminator and a content adversarial classifier. Encoders are along the same structure of [10]. The content encoder consists of three convolutional layers and four residual blocks. The style encoder consists of four convolutional layers and a fully connected layer. The structure of the generator and the content encoder is symmetrical, consisting of four residual blocks and three transposed convolutions. The discriminator and the content adversarial classifier both adopt the structure of PatchGAN [5], which is composed of four layers of convolution and the discriminator uses a multi-scale structure. During training, use mini-batch stochastic gradient descent (batch size is 4) and Adam optimization algorithm ($\beta_1 = 0.5$, $\beta_2 = 0.999$). The initial learning rate is 0.0001 and the learning rate is reduced by half every 10,000 iterations. Among all experiments, images are randomly cropped to the size of 256×256 as input. The model hyperparameters are specifically set as: $\lambda_{adv} = 1$, $\lambda_{adv_c} = 10$, $\lambda_{recon_x} = 10$, $\lambda_{recon_c} = 1$, $\lambda_{regre} = 20$, $\lambda_{cc} = 0.1$.

The detailed network structure is shown in the Table. 1.

4.3 Detailed Analysis

In this section, we provide a qualitative comparison of our model results with SOTA and an in-depth analysis of disentanglement effects, concluding with a description of the role and irreplaceability of each sub-module based on ablation studies

TABLE 1: Network structure. N, K, S respectively represent the number of channels of the convolution layer, the size of the convolution kernel, and the stride of the convolution. RESBLK stands for Residual Block (Residual Block)

Layer	Content Encoder	Layer Info.
1	CONV	N64,K7,S1
2	CONV,RELU	N128,K4,S2
3	CONV,RELU	N128,K4,S2
4	RESBLK,RELU	N256,K3,S1
5	RESBLK,RELU	N256,K3,S1
6	RESBLK,RELU	N256,K3,S1
7	RESBLK,RELU	N256,K3,S1

Layer	Style Encoder	Layer Info.
1	CONV,RELU	N64,K7,S1
2	CONV,RELU	N128,K4,S2
3	CONV,RELU	N256,K4,S2
4	AdaptiveAvgPool	Output=1
5	CONV,Sigmoid	N8,K1,S1

Layer	Generator	Layer Info.
1	RESBLK,RELU	N256,K3,S1
2	RESBLK,RELU	N256,K3,S1
3	RESBLK,RELU	N256,K3,S1
4	RESBLK,RELU	N256,K3,S1
5	DECONV,RELU	N128,K5,S1
6	DECONV,RELU	N64,K5,S1
7	DECONV,RELU	N3,K7,S1

4.3.1 Evaluation Metrics

We first evaluate generated quality in the aspect of traditional computer graphics: Peak Signal to Noise Ratio (PSNR) and Structural Similarity Index (SSIM). Evaluation indicators based on image depth features are also used e.g. Fréchet Inception Distance (FID) [23], LPIPS Distance [24] and VGG distance.

PSNR is based on the error between corresponding pixel points and is one of the most widely used objective evaluation metrics for images. Larger values indicate less distortion of the generated images.

The basic idea of SSIM is to evaluate the similarity of two images by three aspects: brightness, contrast and structure. SSIM takes values in the range [0,1], with larger values indicating less image distortion.

FID calculates two sets of images' Fréchet Distance on the feature of Inception network [25] to evaluate the similarity of two sets of images. We use it to measure the similarity between the generated images and Ground Truth. The lower FID values mean the generated images are closer to Ground Truth in image level.

The LPIPS distance which is obtained by calculating the weighted Euclidean distance between the depth features of a pair of images is often utilized to measure diversity. Higher LPIPS scores indicate better diversity among the generated images. Similar to the literature [14], experiments in this paper calculates the average LPIPS distance between randomly sampled image pairs from generated haze images to evaluate their diversity.

VGG distance denotes the distance between the VGG [26] feature of the input image and the generated image. Different from FID, VGG distance can better evaluate the similarity between the generated image and Ground Truth in semantic level. When calculating the VGG distance, we use the output of the *pool5* layer of the VGG-19 network as the image feature.



Fig. 4: Multi-level results generated by controlling parameter α . From left to right column, it is obvious that vehicles and trees near vanishing points of the road gradually become invisible as α increases.

4.3.2 Results

In this subsection, we generate multi-level haze images by controlling the fore-mentioned parameter α and compare the proposed model with the current mainstream image translation models including CycleGAN [6], UNIT [9], Pix2Pix [5]. All models are retrained on the training set.

Images with diverse haze level are shown in Fig. 4. Note that we consider the value corresponding to the haze that just emerged to be 0 and the baseline haze to be 1, which refers to haze generated with the atmospheric scattering coefficient β equaling to 1. Then we scale up and down the haze feature in the interval from 0 to 1. From the results, we can tell the difference of haze concentration among images with different parameter α , which indicates that we successfully achieve the distinguishability of produced haze by controlling α . For example, vehicles and trees near vanishing points of the road gradually become indistinguishable as α increases. Under the influence of style feature regression, our networks memorize the distinction between thick and thin haze and learn to generate haze images

without sacrificing the realism.

The qualitative comparison result is shown in Fig. 5. On the whole, there is almost no difference between other methods and this paper, except for the presence of the obvious grid-like stripes in “Pix2Pix”. However, the enlarged area exhibits two different defects. In the first and second rows of images, there appears clear discontinuity at the boundary of haze. The jagged haze boundaries reduce the realism of the generated images. This is mainly because the haze images in our training set (which is reference images) are synthesized based on the atmospheric scattering model, combined with imperfect depth information. Discontinuous deviations in depth images are passed to the reference images. Since other methods only learn the mapping relationship between image domains at the pixel level, their results are inevitably affected by existing error of depth images. In contrast, results of this paper have gradually disappearing haze boundaries which indicates great robustness. The approach in this paper abstracts the haze style from the content to understand the characteristics of the haze and thereby ignoring such probably existing error and generating the

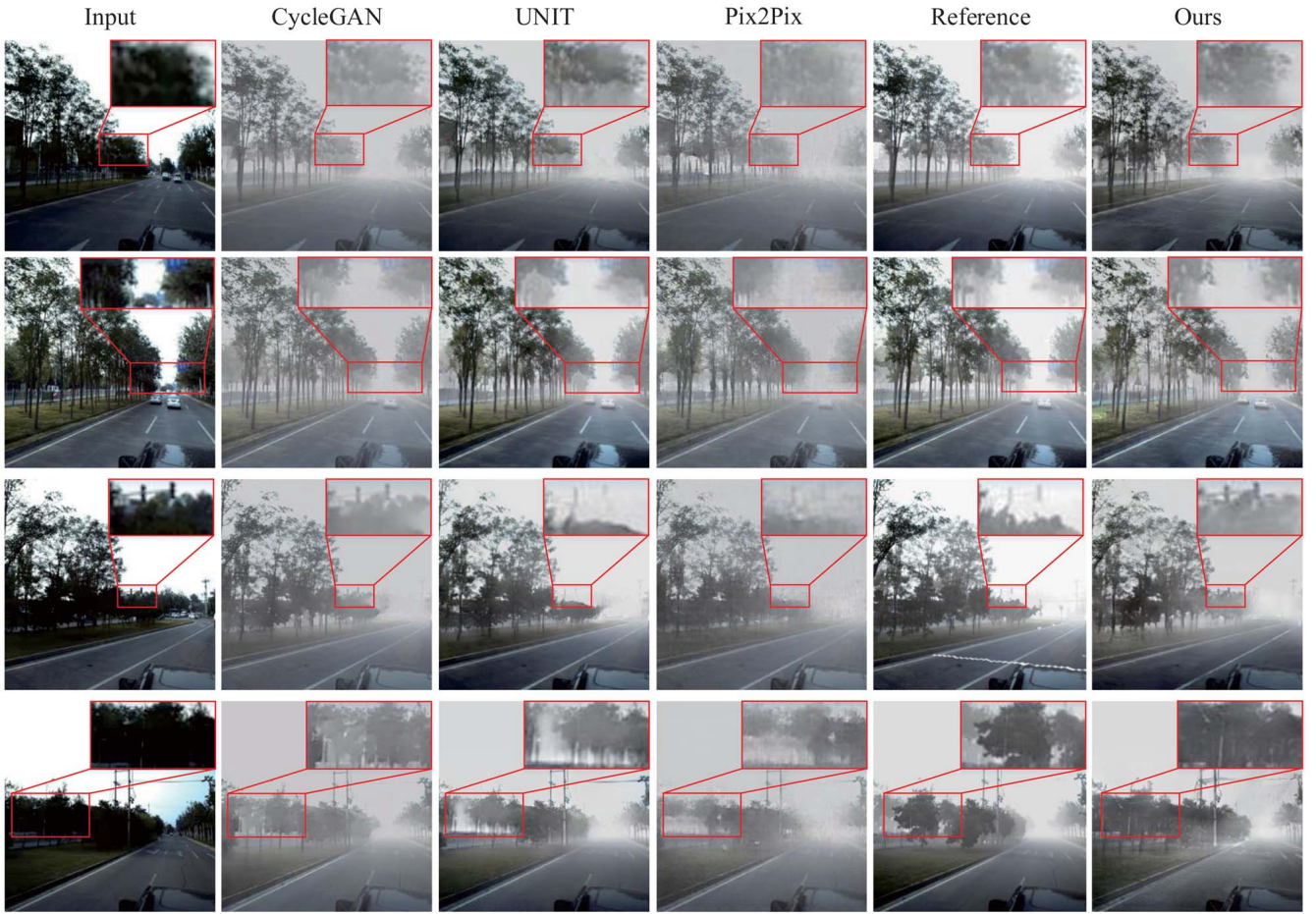


Fig. 5: Subjective comparison results with mainstream methods. The “Reference” column refer to images synthesized via atmospheric scattering model (Eq. 1). Compared to ours, results of other methods have mainly two kinds of flaws which zoomed in inside red boxes. The first two rows of images reflect the discontinuity that occurs at the boundary of synthesized haze, while the next two rows of images indicate the flawed preservation of elements body. Besides, there exists unnatural grid-like stripes in the generated image of supervised method “Pix2Pix”.

continuous, realistic haze. In the third and fourth rows of images produced by other methods, the appearance of image content is corrupted to varying degrees. Take the trees in the enlarged areas as examples, other methods produce truncated trees (the third row shows) or trees blocked by irregular haze (the fourth row shows) whereas the results of our method preserve the structure of the trees in the input image intact. Our method take a disentangled representation learning perspective and better preserve the content of the input image, which further proves its effectiveness.

TABLE 2: Quantitative comparison with baseline methods. d_{VGG} and d_{LPIPS} denote the VGG distance and LPIPS distance respectively. Among them, the smaller the value of d_{VGG} and FID, the better the experimental result. The larger the value of other indicators, the better the experimental result

module	SSIM	PSNR	d_{VGG}	FID	d_{LPIPS}
UNIT	0.552	17.518	0.425	28.138	0.064
CycleGAN	0.586	17.192	0.443	29.665	0.052
Pix2Pix	0.698	18.736	0.291	27.084	0.043
Ours	0.686	18.622	0.321	27.414	0.081

The results of the quantitative comparison further confirm conclusion above. Using the evaluation metrics described in the 4.3.1 section, we quantitatively compare the experimental results from two perspectives of diversity (LPIPS distance) and quality

(SSIM, PSNR, VGG distance, FID distance) of generated images as the Table. 3 shows. From the perspective of image quality, compared with unsupervised methods (UNIT [9], CycleGAN [6]), our method achieves better results based on no matter the traditional evaluation index (PSNR and SSIM) or the index of depth features (VGG distance, FID distance). What is more, similar experimental results are also obtained even compared with the supervised method (Pix2Pix [5]). From the perspective of the diversity of generated images, according to the LPIPS distance, our method is obviously superior to other methods without doubt.

4.3.3 Disentanglement Analysis

Although content features and style features of images are extracted by the content encoder and style encoder respectively and we apply a few constraints to suppress the redundant information in each other, it is not explicit enough to judge whether the model successfully realizes the disentanglement and how completely. Respectively observing extracted feature statics is useless to explain how well the disentanglement works. Instead, we turn to consider what happens if the disentanglement is not effective. Ideally, the content feature of an image should not contain any style information which represents a certain level of haze. In other words, it is impossible to classify whether an image is a haze-free image or a haze image only based on its content feature if the

content feature does not entangle with any style knowledge. On the other hand, using the style feature can directly classify whether the real image belongs to the haze image or the haze-free image. Therefore, we train a classification network with different inputs and evaluate the accuracy on the test set to make a comparison. Experimental results are shown in Table. 3. We firstly use the experiment which inputs the feature extracted by CycleGAN [6] as a control group to indicate the baseline accuracy of classification using entangled features (the fourth column). The classification accuracy rate in content space (the second column) is lower than the base accuracy and close to 0.5 which shows that the network has trouble in classifying which domain the content comes from. On the contrary, the network hardly makes a mistake when using style as criterion (the third column) and performs better compared with directly using image as input (the fifth column). This contrast indicates that the content features disentangled by our model contain almost no domain-related knowledge while the style features convey implicitly exactly the style information used to delineate the image domain, which further confirms the success of our model in disentangling style and content.

TABLE 3: Classification accuracy on different feature spaces

Accuracy	Content	Style	CycleGAN	Image
train set	0.615	0.987	0.875	0.973
test set	0.581	0.972	0.853	0.952

4.4 Ablation Studies

In order to illustrate the role of the various modules of our model and their irreplaceability, we draw on several ablation experiments as follows.

4.4.1 Quantitative Evaluation

TABLE 4: Quantitative comparison results of models obtained after removing different losses. d_{VGG} and d_{LPIPS} indicate the distance of VGG and LPIPS respectively. The smaller the value of d_{VGG} and FID, the better the experimental result. The larger the value of other indicators, the better the experimental result

Module	SSIM	PSNR	d_{VGG}	FID	d_{LPIPS}
removing \mathcal{L}_p	0.662	18.082	0.313	32.134	0.064
removing \mathcal{L}_{KL}	0.639	17.624	0.293	29.414	0.163
removing \mathcal{L}_{adv}	0.669	18.262	0.284	32.245	0.147
removing \mathcal{L}_{cc}	0.438	14.201	0.728	40.620	0.106
complete model	0.686	18.622	0.321	27.414	0.081

We obtain three variant models by removing the adversarial classification loss \mathcal{L}_{adv} , cross-cycle consistency loss \mathcal{L}_{cc} and content perception similarity loss \mathcal{L}_p . These three models and the complete model are analyzed from a quantitative and qualitative perspective and it is found that the performance of the complete model is the best.

Table. 4 is the PSNR, SSIM, VGG distance, FID, LPIPS distance of experimental results of each variant model and Fig. 6 are haze images generated by them, respectively. According to the Table. 4, we can see that removing \mathcal{L}_{recon} and \mathcal{L}_{cc} obviously reduced the quality of generated images. The comparison between Fig. 6a and Fig. 6e also confirms that. This shows that one-way loss constraint cannot produce a high-quality image, which is consistent with the discovery of CycleGAN [6]. In addition, removing \mathcal{L}_{adv} (Fig. 6c) decreases the quality of output images to varying degrees, which shows that both are necessary to the

process of disentanglement. According to the Table. 4, it can be found that removing \mathcal{L}_{cc} and \mathcal{L}_{adv} will both increase LPIPS which indicates that the diversity of generated images increases. However, that is not the result we want since it is not the increase in the diversity of haze, but the change in the content of generated haze images. It has been explained in 3.2.3 that the model without cycle consistency loss constraint will map the input haze-free image to any haze image and there is no guarantee that the content of the generated image is consistent with the input image. As a result, content of the generated image produced by the same haze-free image differs each time. Meanwhile, the removal of \mathcal{L}_{KL} and \mathcal{L}_{adv} will relax the constraints on haze and content characteristics which leads to the failure of the disentanglement of the content feature and the haze feature. It results in the haze feature containing the content information of the haze image and the content of each generated image is affected by the haze characteristics. By comparing the Fig. 6d and Fig. 6e, it is obvious that applying \mathcal{L}_p can effectively reduce the composite traces of generated images and improve their quality. It is worth noticing that the FID value of the complete model is quite different from other variant models. In other words, the overall distribution of the haze image generated by the complete model is the closest to Ground Truth.

4.4.2 Ablation Study on the Self-supervised Style regression

Like previously elaborated, the transmittance map $t(x)$ of the image plays a major influence in the haze rendering process. For our extracted style features to be a certain form of mapping to it and not contain redundant content information, we propose the self-supervised style regression. Fig. 7 visualizes the impact of this operation on the feature maps learned by the network. The pictures of 3^{rd} -layer refer to the outputs of the third layer of the generator. We can see from the picture that after inputting the extracted style features into the generator, they can be decoded into such feature maps which are similar to transmittance map of the scenes. This indicates that the style features we extracted can be viewed as the latent transmittance maps of input images. It is obvious from the results that in the absence of self-supervised style regression, the feature maps obtained from the decoding of the style features is basically a clear description of the entire scene content, which indicates that the style features extracted by the network also contain redundant content information such as the edges of the scene. The quality of generated haze hence compromised. Conversely, the scene structure in the feature map becomes blurred under the constraints of self-supervised regression. This shows that the style encoder focuses more on extracting haze-related style features and reducing the extracted content information when encoding and further proves the effectiveness of our method.

4.4.3 Ablation Study on the Shared Style Encoder

To ensure that the resulting haze is distributed in the right places, we use a shared style encoder in our model. We hope that the haze-free images can provide an essential understanding of spatial structure of scenes to haze-related style features extracted from haze images. To verify this, we set up the following experiment for comparison: two separate style encoders are used to extract the style features for the haze-free images and the haze images, respectively.

Results are shown in Fig. 8. From the images we can tell that compared to using a shared style encoder, the model with

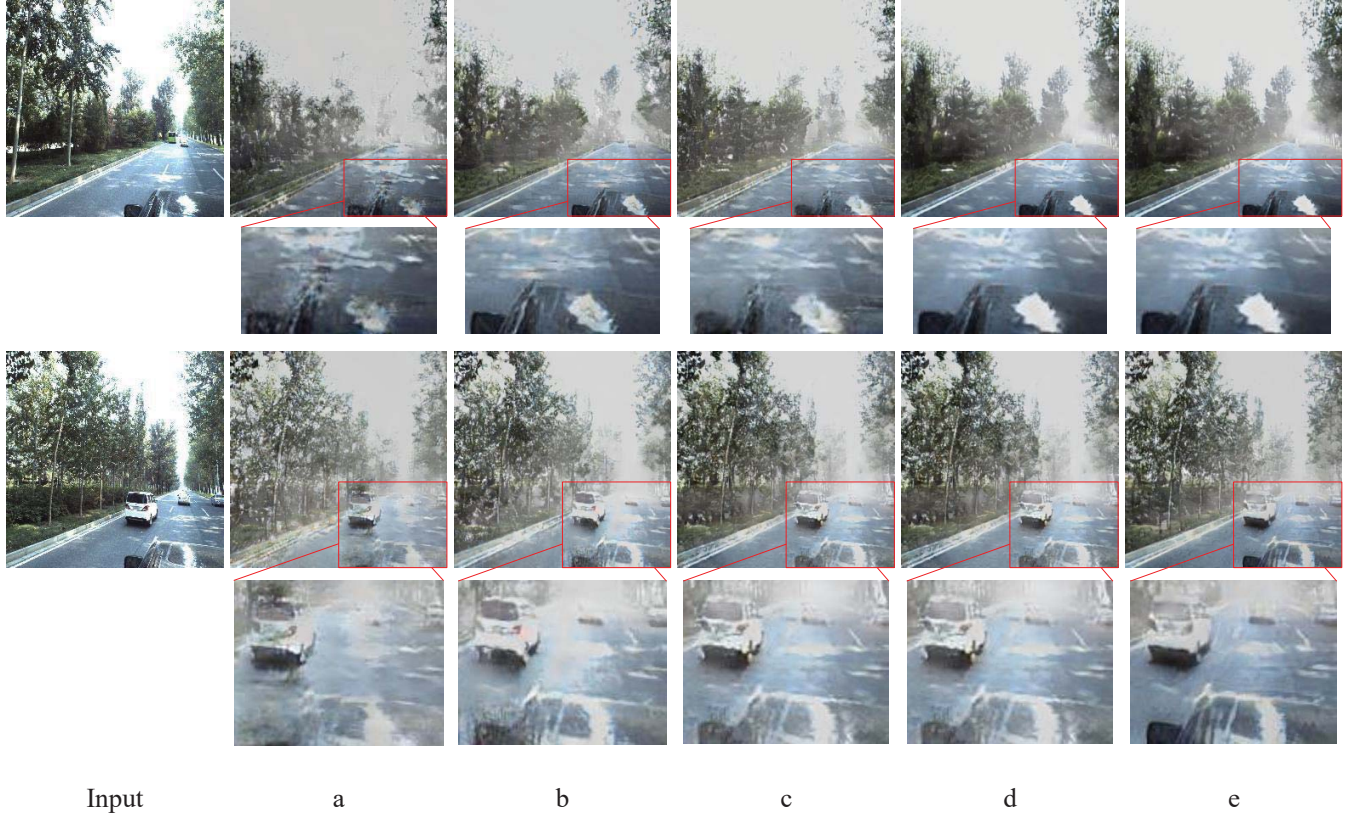


Fig. 6: Comparison of experimental results. (a) represents the result of removing \mathcal{L}_{recon} , (b) represents the result of removing \mathcal{L}_{KL} (c) represents the result of removing \mathcal{L}_{adv} , (d) represents the result of removing \mathcal{L}_p , (e) represents the result of the complete method

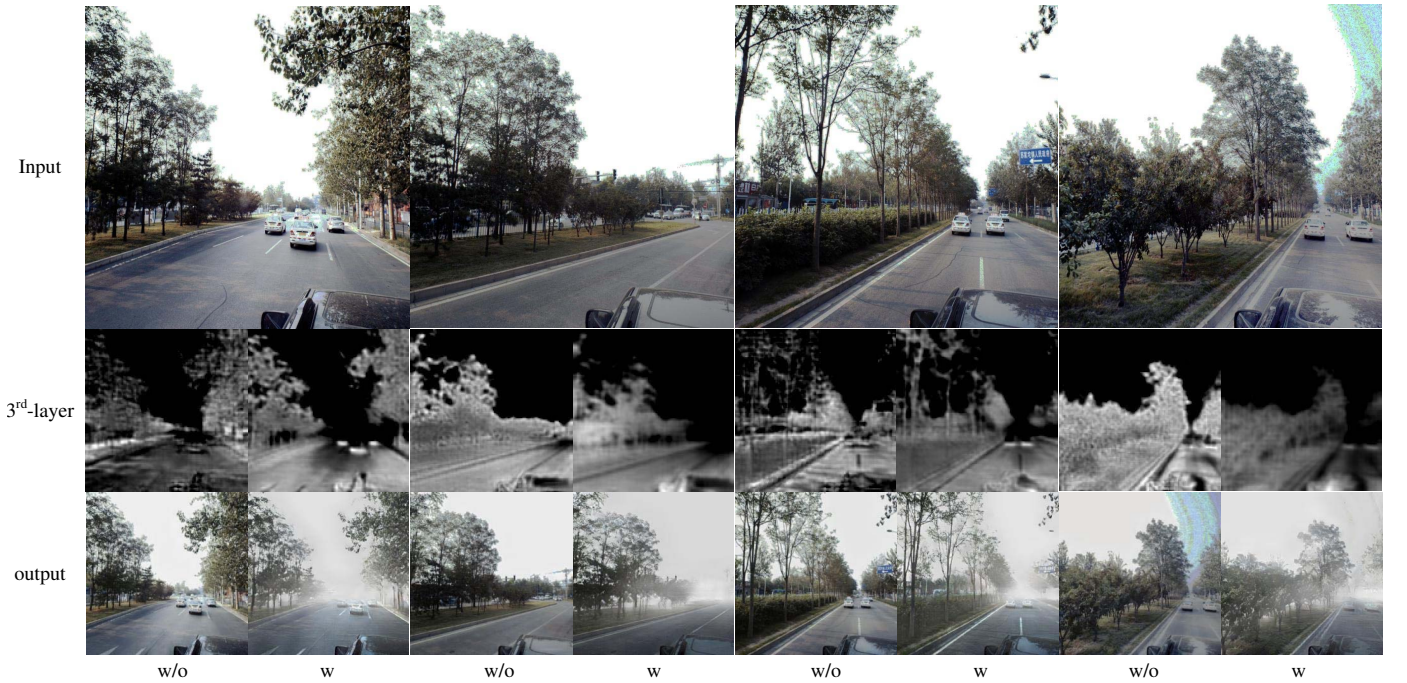


Fig. 7: Visual comparisons of latent transmittance map with and without the process of self-supervised style regression. The first row is the input images. Images in the second row are the outputs of the third layer of our generator and corresponding results are in the last row. Vertically, columns with index “w/o” are experiments results without self-supervised style regression and “w” columns are the opposite.

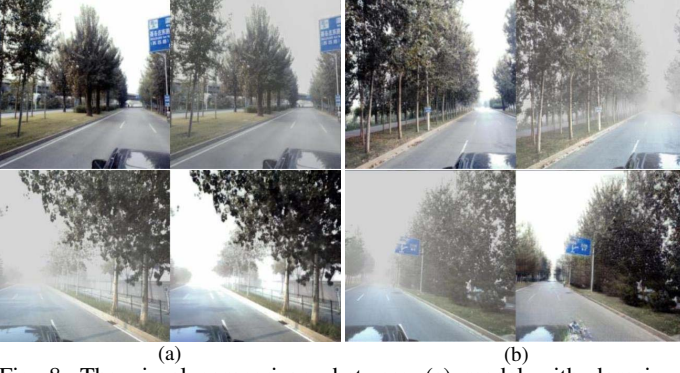


Fig. 8: The visual comparisons between (a) model with domain-specific style encoders and (b) model with shared style encoder. The first row are images of the process of adding haze while the second row shows outputs during dehazing.

domain-specific style encoders is only able to add a uniform luminance, which indicates that the disentanglement of content and style is degraded. Due to such incomplete disentanglement, parts of scenes' prior knowledge that the content encoder should have learned is missing so the model fails to generate elements at the vanishing point of the road in the dehazing process. In the opposite, applying a shared style encoder to both image domains ensures that encoders fully utilize all samples from two domains and realize the successful disentanglement.

5 SIGNIFICANCE IN SCENARIO TESTING FOR AUTONOMOUS DRIVING

To sufficiently and profoundly demonstrate that the haze images generated by our method provide sufficient and effective difficult scenario data support for the scenario test of the autonomous driving perception module, we set up three sets of experiments to explore the distribution change regularity and correlation of the worst perception scenario (WPS) in the dataset before and after the addition of the generated haze images, and the rationality of generating the images with controllable haze density for controlling the difficulty of scenario. In this work, based on the framework of the worst perception scenario search proposed in our previous work, we use YOLOv3 to conduct the worst perception scenario search experiments for vehicle detection on the ApolloScape.

5.1 The regularity of the distribution changes of the worst scenario

From the ApolloScape, we choose the continuous road scenario data as the original dataset, a total of 5773 data, all of which contain vehicles. Subsequently, we use the original dataset to generate the corresponding 5773 haze images with the highest haze level, and combine the original image and the generated image into a haze dataset, a total of 11574 images. Notice that the resolution of the generated image is inconsistent with the resolution of the original image, we need to downsample the original data to eliminate the influence of image quality on the results of search experiments. Considering that the resolution is greatly reduced, we filter the labels of the processed data by eliminating the bounding boxes with a length and width less than 5 pixels.

Combining the scenario annotation from the dataset and image coding from our encoder, we design a scenario search space

TABLE 5: F1 score of the test scenario on two datasets, including the comparison of the overall average performance, the average performance of all the worst scenes and the performance of the worst scenes found.

Dataset	Avg of all data	Avg of WPS	Worst
Original dataset	0.6022	0.3665	0.1654
Haze dataset	0.4641	0.0906	0

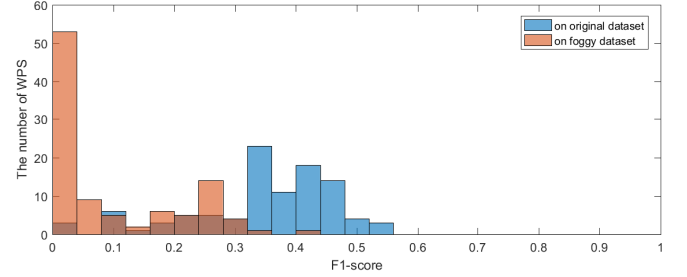


Fig. 9: The performance distribution diagram of the WPS searched on the two datasets.

consisting of 5 scenario-level feature parameters (number of motor vehicles, number of pedestrians, number of non-motor vehicles, number of people, and haze level code) and 25-dimensional content coding obtained by content encoder (Reducing the dimensionality of content coding to 25 dimensions through the PCA algorithm). In particular, the haze level code has two values of 0 and 1 in the haze dataset, but only 0 in the original dataset. For the configuration of the framework of the worst perception scenario search, we set the number of iterations for each search to 300, and perform 100 search experiments on the original dataset and the haze dataset respectively.

Table 5 shows the comparison between the overall performance and the performance of the worst perception scenario in the two datasets. Intuitively, the overall performance of the perception algorithm on the haze dataset has dropped significantly compared to the original dataset, and this trend is also manifested in the worst perception scenario. This result shows that the addition of generating haze images has significantly improved the difficulty of the dataset, and this improvement is consistent, not only for simple scenarios, but also for the worst perception scenarios. As shown in Fig. 9, the change in the performance distribution of the worst perception scenario shows the promotion of increasing the upper limit of the difficulty of the worst scenario in the dataset.

5.2 The correlation of the distribution changes of the worst scenario

Based on the above experimental search results, we design a transfer experiment to prove the correlation between the worst perception scenarios on the two datasets.

Concretely, since the haze level code in the search space has one value in the original dataset, we can directly transfer the remaining scenario parameters of the worst perception scenario from the haze dataset to the original dataset to complete the data matching of the scenario and performance testing. As shown in Fig. 10, we find that most of the worst scenarios on the haze dataset are simple scenarios in the original dataset, whose performance distribution became quite uniform. We preliminarily believe that the result is that the generation of haze images makes the simple scenarios of the original dataset performance degraded under the control of haze factors. It shows that generating haze

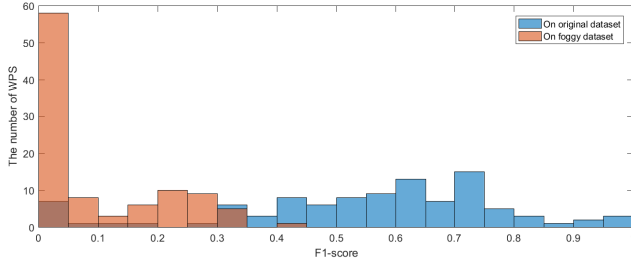


Fig. 10: The experimental results of transferring the WPS of the haze dataset to the original dataset.

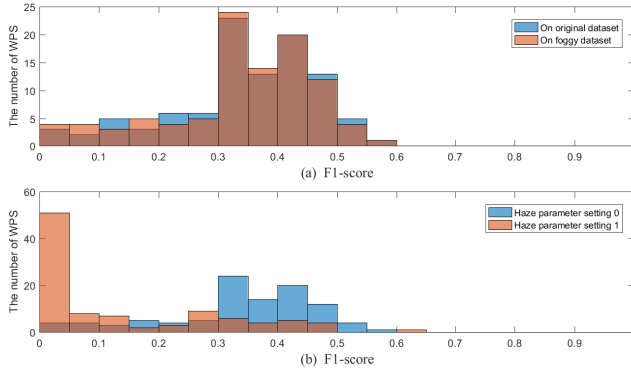


Fig. 11: The experimental results of transferring the WPS of the original dataset to the haze dataset. The performance distribution changes of all scenario parameters remain unchanged (the haze level code is always 0) are plotted in a. The scenario parameters except the haze level code remain unchanged (the haze level code is set to 1), and the performance distribution changes are plotted in b.

images plays an important role in enhancing the richness of difficult scenarios in the dataset.

In turn, the worst perception scenarios on the original dataset are directly transferred to the haze dataset. As expected, since the haze dataset contains the original dataset, Fig. 11 shows that the performance distribution on the two datasets is the same. Based on the worst perception scenario in the original dataset, we also implement a comparative experiment in which the haze level code is reversed while other scenario parameters remain unchanged. Different from the result of direct transfer, the performance degradation becomes obvious as shown in Fig. 11. Combining the above two comparisons, we believe that the worst scenarios in the haze dataset include worst scenarios in the original dataset and haze has increased the difficulty level of such scenarios.

5.3 The correlation between haze density and the difficulty of scenario set

To explore the effect of controllable haze level on scenario testing, based on the original dataset, we have added various generated images of different haze level, including 0.25, 0.5, 0.625, 0.75, 0.875, 1. The data processing method is consistent with the above experiment, then we can get a new dataset of different haze level composed of 40,411 images, which is called the multiple haze dataset here.

The scenario search space maintains the previous configuration, but the haze level code, one of the scenario-level feature parameters, needs to be converted from (0, 1) to (0, 0.25, 0.5, 0.625, 0.75, 0.875, 1). We set the number of iterations for each

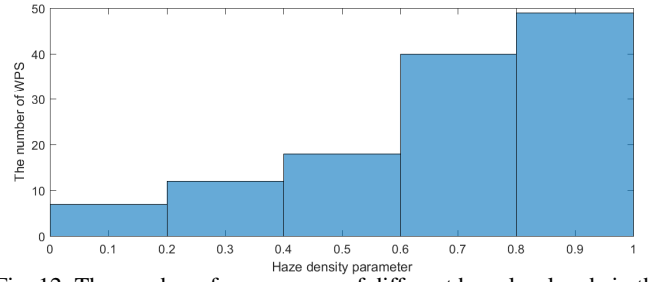


Fig. 12: The number of occurrences of different haze level code in the 125 WPSs searched on the multiple haze dataset.

TABLE 6: Pearson correlation coefficient between scenario-level parameter values and the frequency of WPS.

Scenario-level parameter	Pearson correlation coefficient
Vehicle	-0.4570
Person	0.2606
Non-motor	-0.5479
Group	-0.3134
Haze	0.8396

search to 300, and perform 125 search experiments on the multiple haze dataset.

As shown in Fig. 12, the haze level code of the worst perception scenarios obtained by the search are mainly distributed in the high level range. Therefore, we conclude that the change in haze level may be positively correlated with the degree of influence of scene difficulty.

Based on the fact that the higher the frequency of occurrence of the parameter value in the worst perception scenario, the greater the degree of influence, we use the Pearson coefficient of the scenario parameter value and the frequency of the parameter to measure the correlation between the scenario parameter and the worst perception scenario. In table 6, we calculated the correlation of 5 scenario-level parameters. In previous work, it was found that traffic participants such as the number of vehicles and pedestrians should be strongly correlated with the worst perception, but the correlation here is relatively weak, or even negative. We believe that it should be the decorrelation caused by the elimination of the true value of the small target after the data resolution has decreased. The influence of haze level code shows a strong linear correlation, which provides a reasonable and reliable experimental basis for us to change the haze level code to achieve adaptive difficulty transformation of scenario testing.

6 CONCLUSION

This paper proposes a level-aware haze image generation method based on disentangled representation learning. By randomly setting the haze level of generated image, we successfully disentangle the haze style and content feature in a self-supervised manner. In order to learn the mapping from haze-free images to haze images, this paper uses the cycle consistency loss to narrow the implicit space. Besides, we conduct comparative experiments to analyze the impact of each loss or module in the model on the result. Compared with other methods quantitatively and qualitatively, results all indicate that our method can generate high-quality and high-diversity traffic scene images in haze. Finally, we demonstrate the obvious negative impact of haze on specific task by performing worst scenario searching, which proclaims the significance in the generation of haze scenes for autonomous driving testing.

APPENDIX

In this appendix, we provide a derive of Eq. 5. Neural networks are widely utilized to learn the inference process $h : O \rightarrow Z$ leading from observations to latent space representations. Suppose that we have a group G of manipulations on O via an action $\cdot : G \times O \rightarrow O$. According to the definition in [27], what disentangled representations do is to realize the corresponding manipulations through action $\cdot : G \times Z \rightarrow Z$ and reflect such manipulation in O . This requires that action g should commute with f :

$$g \cdot f(o) = f(g \cdot o), \forall g \in G, o \in O \quad (19)$$

In our case, the inference process are the content and style encoders. Suppose that there are o_1 from clear image domain and o_2 from haze image domain. o_1 and o_2 have style features s_1, s_2 and content feature c_1, c_2 . Specifically, we refer f to the style encoder. Our purpose is to train the style encoder to extract well disentangled style feature:

$$f(o_1) = s_1, f(o_2) = s_2 \quad (20)$$

In the self-supervised style regression process, we interpolate the style features extracted from the two images to obtain s :

$$s = \alpha f(o_1) + (1 - \alpha) f(o_2) \quad (21)$$

According to Eq. 19, the action of interpolating should correspond to that action on O . Then we have:

$$s = f(\alpha o_1 + (1 - \alpha) o_2) \quad (22)$$

REFERENCES

- [1] C. Sun, B. Kong, L. He, and Q. Tian, "An algorithm of imaging simulation of fog with different visibility," in *2015 IEEE International Conference on Information and Automation*. IEEE, 2015, pp. 1607–1611.
- [2] A. Sarker, M. Akter, and M. S. Uddin, "Simulation of hazy image and validation of haze removal technique," *Journal of Computational Chemistry*, vol. 07, no. 2, pp. 62–72, 2019.
- [3] T. Mallick, P. P. Das, and A. K. Majumdar, "Characterizations of noise in kinect depth images: A review," *IEEE Sensors journal*, vol. 14, no. 6, pp. 1731–1740, 2014.
- [4] C. Sweeney, G. Izatt, and R. Tedrake, "A supervised approach to predicting noise in depth images," in *2019 International Conference on Robotics and Automation (ICRA)*. IEEE, 2019, pp. 796–802.
- [5] P. Isola, J.-Y. Zhu, T. Zhou, and A. A. Efros, "Image-to-image translation with conditional adversarial networks," in *Proceedings of the IEEE conference on computer vision and pattern recognition*, 2017, pp. 1125–1134.
- [6] J. Y. Zhu, T. Park, P. Isola, and A. A. Efros, "Unpaired image-to-image translation using cycle-consistent adversarial networks," in *IEEE International Conference on Computer Vision*, 2017, pp. 2242–2251.
- [7] P. Wenzel, Q. Khan, D. Cremers, and L. Leal-Taixé, "Modular vehicle control for transferring semantic information between weather conditions using gans," *arXiv preprint arXiv:1807.01001*, 2018.
- [8] X. Huang, M.-Y. Liu, S. Belongie, and J. Kautz, "Multimodal unsupervised image-to-image translation," in *Proceedings of the European Conference on Computer Vision (ECCV)*, 2018, pp. 172–189.
- [9] M.-Y. Liu, T. Breuel, and J. Kautz, "Unsupervised image-to-image translation networks," *arXiv preprint arXiv:1703.00848*, 2017.
- [10] H.-Y. Lee, H.-Y. Tseng, J.-B. Huang, M. Singh, and M.-H. Yang, "Diverse image-to-image translation via disentangled representations," in *Proceedings of the European Conference on Computer Vision (ECCV)*, 2018, pp. 35–51.
- [11] E. L. Denton *et al.*, "Unsupervised learning of disentangled representations from video," in *Advances in neural information processing systems*, 2017, pp. 4414–4423.
- [12] S. Zhuo and T. Sim, "Defocus map estimation from a single image," *Pattern Recognition*, vol. 44, no. 9, pp. 1852–1858, 2011.

- [13] F. Guo, J. Tang, and X. Xiao, "Foggy scene rendering based on transmission map estimation," *computer games*, vol. 2014, p. 10, 2014.
- [14] J. Zhu, R. Zhang, D. Pathak, T. Darrell, A. A. Efros, O. Wang, and E. Shechtman, "Toward multimodal image-to-image translation," *neural information processing systems*, pp. 465–476, 2017.
- [15] Y. Choi, M. Choi, M. Kim, J.-W. Ha, S. Kim, and J. Choo, "Stargan: Unified generative adversarial networks for multi-domain image-to-image translation," in *Proceedings of the IEEE conference on computer vision and pattern recognition*, 2018, pp. 8789–8797.
- [16] A. H. Liu, Y.-C. Liu, Y.-Y. Yeh, and Y.-C. F. Wang, "A unified feature disentangler for multi-domain image translation and manipulation," in *Advances in neural information processing systems*, 2018, pp. 2590–2599.
- [17] M. F. Mathieu, J. J. Zhao, J. Zhao, A. Ramesh, P. Sprechmann, and Y. LeCun, "Disentangling factors of variation in deep representation using adversarial training," in *Advances in Neural Information Processing Systems*, 2016, pp. 5040–5048.
- [18] X. Chen, Y. Duan, R. Houthoofd, J. Schulman, I. Sutskever, and P. Abbeel, "Infogan: Interpretable representation learning by information maximizing generative adversarial nets," in *Advances in neural information processing systems*, 2016, pp. 2172–2180.
- [19] X. Yu, Y. Chen, T. Li, S. Liu, and G. Li, "Multi-mapping image-to-image translation via learning disentanglement," *arXiv preprint arXiv:1909.07877*, 2019.
- [20] Q. Chen and V. Koltun, "Photographic image synthesis with cascaded refinement networks," in *Proceedings of the IEEE International Conference on Computer Vision*, 2017, pp. 1511–1520.
- [21] Y. Taigman, A. Polyak, and L. Wolf, "Unsupervised cross-domain image generation," *arXiv preprint arXiv:1611.02200*, 2016.
- [22] X. Huang, X. Cheng, Q. Geng, B. Cao, D. Zhou, P. Wang, Y. Lin, and R. Yang, "The apolloscape dataset for autonomous driving," in *Proceedings of the IEEE Conference on Computer Vision and Pattern Recognition Workshops*, 2018, pp. 954–960.
- [23] M. Heusel, H. Ramsauer, T. Unterthiner, B. Nessler, and S. Hochreiter, "Gans trained by a two time-scale update rule converge to a local nash equilibrium," *neural information processing systems*, pp. 6626–6637, 2017.
- [24] R. Zhang, P. Isola, A. A. Efros, E. Shechtman, and O. Wang, "The unreasonable effectiveness of deep features as a perceptual metric," in *Proceedings of the IEEE conference on computer vision and pattern recognition*, 2018, pp. 586–595.
- [25] C. Szegedy, V. Vanhoucke, S. Ioffe, J. Shlens, and Z. Wojna, "Rethinking the inception architecture for computer vision," *computer vision and pattern recognition*, pp. 2818–2826, 2016.
- [26] K. Simonyan and A. Zisserman, "Very deep convolutional networks for large-scale image recognition," *Computer Science*, 2014.
- [27] I. Higgins, D. Amos, D. Pfau, S. Racaniere, L. Matthey, D. Rezende, and A. Lerchner, "Towards a definition of disentangled representations," *arXiv preprint arXiv:1812.02230*, 2018.



Chi Zhang (S'14-M'20) received the B.E. degrees from the Xi'an Jiaotong University, Xi'an, China, in 2011. He is currently a Ph.D. Candidate with the College of Artificial Intelligence, Xi'an Jiaotong University, Xi'an, China. His research interests are focused on intelligence evaluation for autonomous vehicle. He is a member of the IEEE.



Zihang Lin received the B.E. degrees from the Xi'an Jiaotong University, Xi'an, China, in 2020. He is currently a M.D. Candidate with the College of Artificial Intelligence, Xi'an Jiaotong University, Xi'an, China. His research interests are focused on intelligence evaluation for autonomous vehicle, computer vision and graphics.



Gaofeng Meng received the B.S. degree in applied mathematics from Northwestern Polytechnical University, Xi'an, China, in 2002, and the M.S. degree in applied mathematics from Tianjin University, Tianjin, China, in 2005, and the Ph.D. degree in control science and engineering from Xi'an Jiaotong University, Xi'an, China, in 2009. He is currently an Associate Professor with the National Laboratory of Pattern Recognition, Institute of Automation, Chinese Academy of Sciences, Beijing, China. His research interests include document image processing and computer vision. He is an Associate Editor for Neurocomputing.



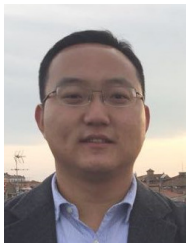
Liheng Xu received the B.E. degrees from University of Electronic Science and Technology of China, Chengdu, China, in 2019. He is currently a M.D. Candidate with the College of Artificial Intelligence, Xi'an Jiaotong University, Xi'an, China. His research interests are focused on intelligence evaluation for autonomous vehicle, computer vision and graphics.



ZongLiang Li received the B.E. degree and M.E. degree from the Xi'an JiaoTong University, Xi'an, China. His research interests are focused on image synthesis for the evaluation of autonomous vehicle, computer vision and graphics.



Li Li (S'05–M'06–SM'10–F'17) is currently an Associate Professor with the Department of Automation, Tsinghua University, Beijing, China, working in the fields of artificial intelligence, intelligent control and sensing, intelligent transportation systems, and intelligent vehicles. He serves as an Associate Editor of IEEE Transactions on Intelligent Transportation Systems, a Member of Editorial Advisory Board for Transportation Research Part C: Emerging Technologies and ACTA Automatica Sinica.



Le Wang (M'14–SM'20) received the B.S. and Ph.D. degrees in Control Science and Engineering from Xi'an Jiaotong University, Xi'an, China, in 2008 and 2014, respectively. He is currently an Associate Professor with the College of Artificial Intelligence of Xi'an Jiaotong University, Xi'an, China. His research interests include computer vision, machine learning, and their application for web images and videos. He is a Senior member of the IEEE.



Nanning Zheng (SM'93–F'06) graduated from the Department of Electrical Engineering, Xi'an Jiaotong University, Xi'an, China, in 1975, and received the M.S. degree in information and control engineering from Xi'an Jiaotong University in 1981, and the Ph.D. degree in electrical engineering from Keio University, Yokohama, Japan, in 1985. He joined Xi'an Jiaotong University in 1975, and he is currently a Professor and the Director of the College of Artificial Intelligence. His research interests include computer vision,

pattern recognition and image processing, and hardware implementation of intelligent systems.



Yuehu Liu received the B.E. and M.E. degrees from the Xi'an Jiaotong University, Xi'an, China, in 1984 and 1989, respectively, and the Ph.D. degree in electrical engineering from Keio University, Tokyo, Japan, in 2000. He is currently a professor with Xi'an Jiaotong University. His research interests are focused on computer vision, computer graphics, and simulation testing for autonomous vehicle. He is a member of the IEEE and the IEICE.